

Point Defect-Induced UV-C Absorption in Aluminum Nitride Epitaxial Layers Grown on Sapphire Substrates by Metal-Organic Chemical Vapor Deposition

Nadine Tillner, Christian Frankerl,* Felix Nippert, Matthew J. Davies, Christian Brandl, Rainer Lösing, Martin Mandl, Hans-Jürgen Lugauer, Roland Zeisel, Axel Hoffmann, Andreas Waag, and Marc Patrick Hoffmann

Herein, the optical properties of aluminum nitride (AlN) epitaxial layers grown on sapphire substrates by metal-organic chemical vapor deposition (MOCVD) are reported. The structures investigated in this study are grown at highly different degrees of supersaturation in the MOCVD process. In addition, both pulsed and continuous growth conditions are employed and AlN is deposited on nucleation layers favoring different polarities. The samples are investigated by photoluminescence (PL), photoluminescence excitation (PLE), and absorption spectroscopy and are found to vary significantly in absorption and emission characteristics. Two distinct absorption bands in the UV-C spectral range are observed and examined in greater detail, with either giving rise to a significant absorption coefficient of around 1000 cm^{-1} . The corresponding defect transitions are identified by PL spectroscopy. Combined with secondary-ion mass spectrometry (SIMS) measurements, these absorption bands are allocated to the incorporation of carbon and oxygen impurities, depending on the applied growth conditions. Furthermore, similarities with other epitaxial growth techniques serving as basis for UV-C applications are highlighted. These results are highly relevant for a better understanding of absorption issues in AlN templates grown by various deposition techniques. In addition, consequences for the growth of efficient UV-C devices by MOCVD on sapphire substrates are outlined.


1. Introduction

Efficient light sources emitting in the UV-C spectral range are required for a broad range of medical applications, such as disinfection and water purification.^[1–3] Widespread pathogenic microorganisms are efficiently treated by exposure to UV-C radiation,^[4–6] most commonly generated by high-pressure germicidal lamps which are based on mercury and emit broadband UV-C radiation. Ongoing research efforts on the ultra-wide-bandgap AlGaN material system are anticipated to result in the development of efficient, low-cost, and environmentally friendly light emitting diodes (LED), which are expected to replace mercury-vapor lamps as the main UV-C emission source in the near future.^[7]

However, several fundamental limitations of current AlGaN-based LED devices must be overcome first, until their electrical-to-UV-C power conversion efficiency can compete with that of germicidal lamps. The external quantum efficiency of current devices still remains below 20%^[8]

for multiple reasons, such as poor doping efficiency of p-AlGaN.^[9,10] For this reason, p-GaN is often used as a p-type contact layer, despite fully absorbing UV photons

N. Tillner, C. Frankerl, Dr. M. J. Davies, C. Brandl, Dr. R. Lösing, Dr. M. Mandl, Dr. H.-J. Lugauer, Dr. R. Zeisel, Dr. M. P. Hoffmann
OSRAM Opto Semiconductors GmbH
Leibnizstraße 4, 93055 Regensburg, Germany
E-mail: Christian.Frankerl@osram-os.com

 The ORCID identification number(s) for the author(s) of this article can be found under <https://doi.org/10.1002/pssb.202000278>.

© 2020 The Authors. Published by Wiley-VCH GmbH. This is an open access article under the terms of the Creative Commons Attribution License, which permits use, distribution and reproduction in any medium, provided the original work is properly cited.

Correction added on 19 August 2020, after first online publication: Projekt Deal funding statement has been added.

DOI: 10.1002/pssb.202000278

N. Tillner, Prof. A. Waag
Institut für Halbleitertechnik
TU Braunschweig
Hans-Sommer-Straße 66, 38106 Braunschweig, Germany

C. Frankerl, Dr. F. Nippert, Prof. A. Hoffmann
Institut für Festkörperphysik
Technische Universität Berlin
Hardenbergstraße 36, 10623 Berlin, Germany

Prof. A. Waag
Epitaxy Competence Center
TU Braunschweig
Hans-Sommer-Straße 66, 38106 Braunschweig, Germany

generated in the active area. UV LEDs with top emission therefore suffer from GaN absorption. As a consequence, flip-chip concepts, meaning that the light is extracted through the back-side of the structure, need to be utilized.^[9,11] In this architecture, however, the photons need to pass the whole AlN layer between the sapphire substrate and the active region of the UV LED. The optical quality of the template therefore is of utmost importance.

Typically, AlN epitaxial layers grown on sapphire are used to form a suitable template for UV-C LEDs due to their reasonable lattice matching to Al-rich AlGaIn layers and its large bandgap, avoiding band–band- absorption.^[12] On the downside, AlN epitaxial layers systematically suffer from a considerable concentration of unintentionally incorporated point defects.^[13] Point defects can introduce undesired absorption bands in the UV-C spectral region which significantly deteriorate the light output, as reported for AlN templates on different substrates, for native AlN substrates grown by physical vapor transport (PVT) and AlN grown by hydride vapor phase epitaxy (HVPE).^[14–16] However, the UV-C spectral region is of utmost relevance for medical applications, as the maximum germicidal efficacy for several pathogenic microorganisms^[4–6] is reported at wavelengths close to typical UV-C emission (≈ 250 – 280 nm). This emphasizes the necessity of defect reduction and a thorough study of the absorption related to point defect incorporation in AlN epitaxial layers.

In this study, we examine the relation between absorption and the introduction of point defects into AlN epitaxial layers grown by metal-organic chemical vapor deposition (MOCVD) used for AlN templates on sapphire substrates with varying growth conditions, employing highly different degrees of supersaturation. The vapor supersaturation describes the deviation from the thermodynamic equilibrium during the AlN growth process and serves as a unified parameter to describe the overall growth mode.^[17–19] The individual process parameters, such as the growth temperature and the V/III ratio, define thereby the supersaturation. For example, by increasing the process temperature or lowering the V/III ratio, the vapor supersaturation is decreased, whereas one of the most effective ways to adapt the vapor supersaturation is the growth temperature.^[18,19] In addition, pulsed and continuous growth modes and AlN layers with different polarities are investigated. To analyze the samples, both photoluminescence (PL) and photoluminescence excitation (PLE), and absorption spectroscopy are used as means of investigating the absorption and emission properties of AlN sample structures. In particular, two distinct absorption bands in the UV-C spectral range, in the vicinity of the desired emission wavelength region, could be observed and their dependencies on the used growth conditions and modes are studied. The concentrations of the impurities incorporated into the samples are measured by secondary-ion mass spectrometry (SIMS) and, in combination with the optical response of the structures, an allocation of the absorption bands to the determined types of point defects is proposed. These findings are compared to alternative deposition techniques for heteroepitaxial and homoepitaxial AlN layers (hydride vapor phase epitaxy (HVPE) and physical vapor transport (PVT)), which are all used in high-power UV-C LEDs, despite their widely varying growth procedures. In addition, this article might serve as a guideline to grow transparent AlN epitaxial layers by MOCVD in the UV-C spectral range by carefully adapting growth modes and kinetics.

Table 1. Overview of the samples grown for this study. “+” indicates the continuous growth equivalent, while C2* uses a different nucleation layer compared to sample C2 (see text). The supersaturation values depending of the individual growth conditions are estimated and compared relatively.^[19]

	P	C1	C2	C2*
Temperature [°C]	1330	1150	1420	1420
Metalorganic flow rates [$\mu\text{mol min}^{-1}$]	60	140	140	140
V/III ratio	1216 ⁺	38	38	38
Supersaturation	Medium, $\approx 1 \times 10^4$	High, $\approx 1 \times 10^7$	Low, $\approx 5 \times 10^2$	Low, $\approx 5 \times 10^2$

2. Sample Structure and Measurement Methods

AlN epitaxial layers are deposited in a N_2/H_2 atmosphere with different temperatures and growth parameters on sapphire substrates by MOCVD technique. Trimethylaluminum (TMAI) and ammonia (NH_3) were used as precursors. For all structures, growth was initiated via a few nanometer thick AlN nucleation layer and followed by an $\approx 1.4 \mu\text{m}$ thick high-growth-temperature AlN layer. Four individual samples are grown and studied in this study, with their properties summarized in **Table 1**. The first sample (P) is grown under pulsed growth conditions, while the other samples (C1, C2, C2*) use continuous growth conditions. Sample P is grown at a temperature of 1330°C and a continuous metalorganic flow rate of $60 \mu\text{mol min}^{-1}$ in an NH_3 pulsed mode. Pulsing of NH_3 induces an Al-rich environment supporting III-polar AlN deposition.^[9] The pulsed sequence consists of a 5 s simultaneous growth phase interrupted by a 3 s NH_3 flow pause, generating a continuous equivalent V/III ratio of ≈ 1216 . The samples C1, C2, and C2* are grown under continuous growth conditions with metalorganic flow rates of $140 \mu\text{mol min}^{-1}$ and V/III ratios of ≈ 38 . The growth temperatures vary from 1150°C for sample C1 to 1420°C for samples C2 and C2*, with the only difference between the last two samples being an alternating nucleation layer, which will be described in more detail in the following main paragraph. The detailed process conditions of each sample are additionally unified under the supersaturation as the main growth control parameter, which is estimated by the input parameters, to describe the applied growth mode.^[19] The supersaturation values for the samples P, C1, and C2/C2* are $\approx 1 \times 10^4$, $\approx 1 \times 10^7$, and $\approx 5 \times 10^2$, respectively. As the order of magnitudes of the estimated values are highly different, the supersaturations of the samples P, C1, and C2/C2* are henceforth considered as medium, high, and low, respectively.

Room temperature absorption measurements are performed using a commercial Hamamatsu Quantaurus C9920-02 G system. In this setup, the sample is placed inside a UV-capable integrating sphere and exposed to light of a tunable wavelength between 245 and 400 nm, originating from a 150 W xenon arc lamp connected to a monochromator. After passing through the sample, the residual light is collected and analyzed by a Hamamatsu PMA-12, consisting of a second monochromator coupled to a CCD detector unit. By adjusting the second

monochromator to the original excitation wavelength, errors that may arise through potential defect absorption and re-emission (at lower energies due to Stokes shift) are excluded. As the size, thickness, and surface roughness of all samples do not deviate significantly, reflection coefficients are considered as equal. Therefore, the acquired absorption spectra, generated by calculating the difference of the input and output light intensity at any given wavelength, are believed to be very reliable.

For room temperature PL measurements, a quadrupled Q-switched Nd:YAG laser ($\lambda = 266$ nm) is used as the excitation source. Measurements are performed in a commercial Nanometrics VERTEX-SM-230 PL mapping device. The excitation source for the PLE measurements is a 450 W xenon arc lamp coupled to a two-stage Acton SpectraPro 300i monochromator for wavelength selection. Output light detection is realized by a 0.8 m focal length SPEX 1704 monochromator combined with a Princeton Instruments liquid nitrogen-cooled UV-optimized CCD camera. PLE measurements were performed at $T = 5$ K in a Janis ST-500 cryostat. Low-temperature PLE measurements are preferred for reasons of a sufficient signal-to-noise ratio. SIMS depth profiles were acquired utilizing a Cameca IMS WF magnetic sector instrument using a cesium primary ion beam.

3. Experimental Results and Discussion

In **Figure 1**, the room temperature absorption spectra of samples P, C1, and C2 are shown. Sample P indicates a broad absorption band ranging from below 245–315 nm wavelength with a distinct peak around 265 nm, corresponding to a maximum absorption coefficient of 1053 cm^{-1} . In contrast, the absorption spectra of samples C1 and C2 are almost identical, exhibiting drastically reduced absorption coefficients of 151 cm^{-1} (C1) and 168 cm^{-1} (C2) at an excitation wavelength of 265 nm. The absorption spectrum of these samples is approximately constant across the whole wavelength range studied, without revealing a distinct peak. Measured net absorption at $\lambda = 265$ nm for the samples is $\approx 14\%$ (P), $\approx 2\%$ (C1), and $\approx 3\%$ (C2), respectively. We would like

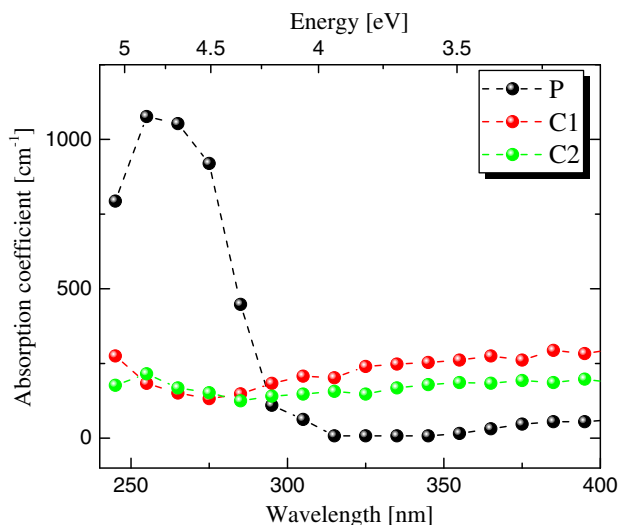


Figure 1. Room temperature absorption spectra of samples P, C1, and C2.

to emphasize here the similarity of the absorption spectra of samples C1 and C2 despite their significant difference in growth temperature (1150°C vs 1420°C) and thus the vapor supersaturation used during the MOCVD process. The absorption of the pulsed-grown sample P, deposited at 1330°C and a medium supersaturation, reveals in contrast a fundamentally different behavior. As the process temperature and therefore the vapor supersaturation of sample P were chosen to be in between those of samples C1 and C2, the apparently deviating defect incorporation into the epitaxially grown film must be a consequence of the NH_3 pulsed growth mode rather than being solely growth-kinetic related. NH_3 pulsing, as used in sample P, is a popular growth technique and is often used to achieve a very low vapor supersaturation or as a technique for multimode AlN growth to lower the threading dislocation density (TDD).^[9] Similar absorption coefficients in the range of 1000 cm^{-1} have been reported for AlN epitaxial layers and native AlN grown by MOCVD, HVPE, or PVT, which are prone to high impurity incorporation originating primarily from oxygen or carbon incorporation.^[14–16] We emphasize here that a UV-C absorption close to 265 nm overlaps with the desired emission wavelength of UV-C LEDs used for disinfection and purification purposes. This finding highlights the need for a more detailed study of the defects accounting for the pronounced absorption band, especially in sample P, which was grown in pulsed growth mode, a method which recently gained popularity in the fabrication of AlN epitaxial layers.

For this reason, resonant PL measurements were performed at room temperature, specifically pumping the absorption band centered around 265 nm due to the choice of excitation source. The obtained spectra are shown in **Figure 2**. Two peaks can be identified in the PL spectrum of sample P, centered at ≈ 310 and 450 nm, as well as the second order peak of 310 nm at 620 nm. Samples C1 and C2 reveal two distinct peaks that are slightly shifted with respect to their positions in sample P, peaking at 325 and 470 nm, respectively. The PL spectra of samples C1

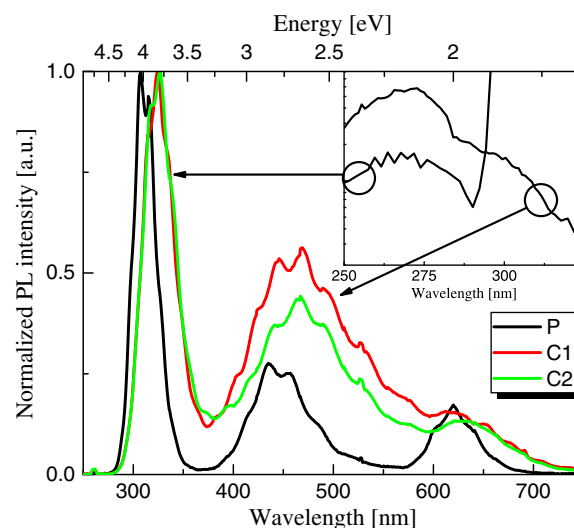


Figure 2. Room temperature PL emission spectra of samples P, C1, and C2. The inset exemplarily shows the PLE spectra recorded at $T = 5$ K of sample P, integrated over the emission bands from 280–350 nm and from 400–500 nm, respectively, as indicated by the black arrows.

and C2 reveal emission peaks at identical energetic positions, coinciding also in shape. This finding leaves no doubt about the similar nature of the point defects incorporated. Here, we cannot exclude that the specific concentration of point defects introduced in samples C1 and C2 varies to some extent, although it appears that the concentration in both samples is too low to induce significant absorption. In addition, the clear energetic shift of the emission peaks of samples C1 and C2 compared to sample P indicates that if the same type of point defects is responsible for the PL emissions in all samples, the defect concentration or their ratio in the latter sample is entirely different. A similar effect, i.e., an energetic PL peak shift depending on the defect concentration, was reported by Collazo et al. for a carbon-related defect in AlN epitaxial layers grown by PVT and HVPE.^[14] We have also performed low-temperature PLE measurements, as exemplarily shown for sample P in the inset of Figure 2. The PLE measurement confirms that the defect emissions centered around 310 and 450 nm originate from the same defect(s) causing the absorption band at 265 nm (cf. Figure 1). The absorption band at 265 nm in sample P may therefore be introduced either by one type of impurity which is incorporated in two different defect states, two different types of impurities, or even three defects in donor–acceptor pair configuration. We note here that the corresponding PLE response is similar for samples C1 and C2, albeit of reduced absolute intensity, altogether indicating a similar defect nature in all three samples, but heavily varying in concentration and therefore absorption behavior depending on the specific growth condition.

Until now, all three samples discussed in this manuscript reveal comparable, smooth surfaces, as clearly observed using differential interference contrast microscopy, indicating a pure III-polar AlN growth. In contrast, sample C2* is grown with the identical high-temperature growth and supersaturation conditions used for sample C2, but on a different underlying nucleation layer, specifically developed to favor a primarily mixed-polar growth (both N- and Al-polar). As a result, the surface morphology of sample C2* is altered and indicates mixed-polar growth with $\approx 15\%$ of the sample being defined by inversion domains. Naturally, the nucleation layer also impacts the subsequent high-temperature AlN deposition. Sample C2* can thus be regarded as a test structure for AlN epitaxial layers utilizing lateral overgrowth of N-polar domains as means of TDD reduction.^[20] As the nucleation layer is found to modify the growth mode of the subsequently grown AlN layer, it may also affect point defect incorporation, e.g., native oxygen incorporation,^[21] and therefore the net absorption in the UV-C energetic range. To study this effect, **Figure 3** directly compares room temperature absorption spectra of samples C2 and C2*, which differ only in the overall polarity determined by the nucleation layer. Sample C2, as already stated in Figure 1, shows an almost constant absorption coefficient of around $150\text{--}200\text{ cm}^{-1}$ over the entire measurement range without a distinct absorption band and a net absorption of 2.5% at $\lambda = 265\text{ nm}$. In contrast, we find a severe increase in UV-C absorption below 320 nm in sample C2*, implying a very broad absorption band with a maximum at a wavelength significantly below 245 nm, exceeding the measurement range of our setup. Here, the absorption coefficient at $\lambda = 265\text{ nm}$ is 927 cm^{-1} with a determined net absorption of 12.5%. The extracted absorption spectrum implies that one or several different types of point

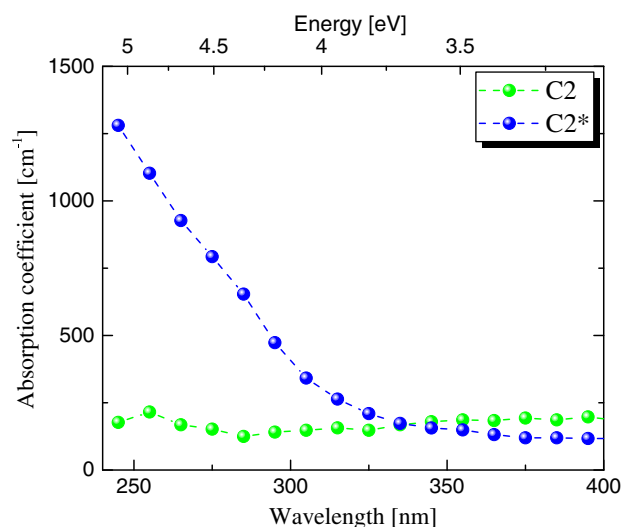


Figure 3. Room temperature absorption spectra of samples C2 and C2*.

defects are predominantly incorporated in sample C2* compared to samples P, C1, and C2, favored by the difference in polarity of the nucleation layer. In general, the emergence of inversion domains during epitaxial growth drastically promotes the incorporating of oxygen,^[21] thus, the interpretation of an oxygen-related absorption band is justified.

To further investigate this change in absorption behavior, resonant PL measurements were conducted on sample C2*, pumping the high-energy flank of the absorption band observed in Figure 3, and compared to the corresponding PL spectra of sample C2. The result is shown in **Figure 4**. As already discussed in Figure 2, the obtained PL spectrum of sample C2 reveals two distinct peaks around 325 and 470 nm. In contrast, only one distinct asymmetric peak centered at 380 nm is observed in the emission spectrum of sample C2*. Therefore, the PL measurements further verify the inherently different nature of the incorporated point defects when altering the nucleation layer.

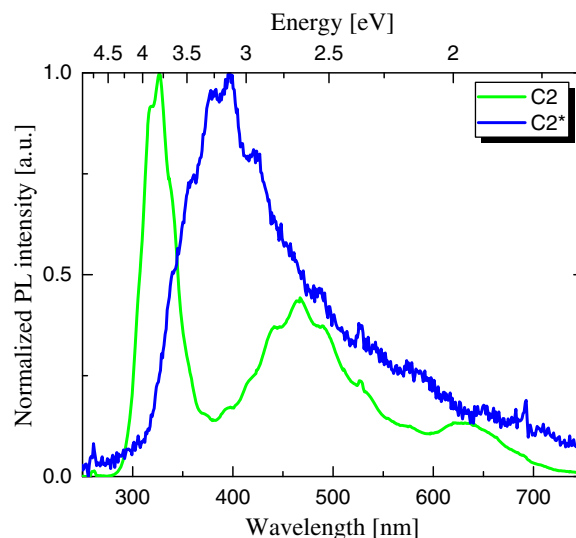


Figure 4. Room temperature PL emission spectra of samples C2 and C2*.

Table 2. Impurity incorporation of silicon, carbon, and oxygen into the samples as determined by SIMS, along with a summary of the observed emission and absorption properties. The supersaturations of the samples are also given to represent the applied growth mode.

	P	C1	C2	C2*
Si [cm^{-3}]	2.2×10^{17}	1.0×10^{16}	3.5×10^{17}	2.5×10^{17}
C [cm^{-3}]	2.0×10^{19}	2.0×10^{17}	1.8×10^{17}	3.0×10^{17}
O [cm^{-3}]	1.3×10^{17}	1.0×10^{17}	9.0×10^{17}	3.0×10^{18}
Supersaturation	Medium, $\approx 1 \times 10^4$	High, $\approx 1 \times 10^7$	Low, $\approx 5 \times 10^2$	Low, $\approx 5 \times 10^2$
PL peak emission [nm]	310/450	325/470	325/470	380
Peak absorption [nm]	265	–	–	<245

To investigate the possible influence of impurity atoms jointly responsible for the observed absorption and PL behavior, we performed SIMS measurements on all samples discussed in this manuscript. Using this method, we were able to reliably determine the respective concentrations of silicon, carbon, and oxygen, which show the foreign atoms most commonly incorporated during the growth process of AlN epitaxial layers by MOCVD. The results are shown in **Table 2**, along with the already discussed emission and absorption properties of the samples, as well as the degrees of supersaturation. We first note that the concentration of Si remains substantially below 10^{18} cm^{-3} for all samples and no clear correlation with the applied growth conditions, the determined absorption coefficients, and the PL emission spectra is found. Therefore, Si can be excluded as the primary source of impurity absorption within the UV-C region in all of the studied samples. The concentration of C is found to be $2.0 \times 10^{19} \text{ cm}^{-3}$ in sample P and only of the order of low 10^{17} cm^{-3} in samples C1, C2, and C2*. As the absorption band centered around 265 nm was only found in sample P and not observed in all other samples, it is unambiguously identified as carbon-related. Our findings are supported by Alden et al. who related the carbon-related defect luminescence at ≈ 320 and ≈ 460 nm to the absorption band at 265 nm in single crystal AlN substrates grown by PVT.^[15] In addition, Collazo et al. also showed a relation between the defect luminescence at ≈ 320 nm and the absorption band at 265 nm for AlN grown by PVT and HVPE.^[14] We highlight the finding that the high incorporation of carbon in our MOVCD-grown AlN layer in sample P is strikingly similar to the incorporation of carbon in PVT-grown AlN native substrates, despite the inherent differences in the growth methods and kinetics of both techniques. Therefore, both approaches serving as a basis of UV-C LEDs—the heteroepitaxial AlN layer on foreign substrates and AlN native substrates for homoepitaxy—suffer from a common defect behavior, affecting the LED performance. Clearly, the near-identical carbon concentration in samples C1 and C2 accounts for the similar absorption and PL emission characteristics of the structures.

In general, the point defect concentration is found to increase with decreasing vapor supersaturation in the growth process.^[22] The vapor supersaturation is defined by the growth parameters, such as the process temperature, the growth rate, and the V/III ratio.^[17,18] Sample P was grown in a medium supersaturation condition with respect to sample C1 (high supersaturation) and C2 (low supersaturation), as relatively estimated by the growth temperature and V/III ratio.^[22] The carbon impurity

concentration is highest in sample P, whereas the highest oxygen impurity is measured for sample C2 (and C2*). Thus, NH_3 pulsing during growth promotes a significant increase in carbon-related point defect concentration. The reason for the substantial incorporation of carbon during pulsed growth is assumed to be an effect of a decomposing SiC carrier at high process temperatures during AlN epitaxy, whereas pulsing gives the opportunity for the impurities to be incorporated. The incorporation of carbon-based defects is more likely than silicon-related defects due to the former's lower point defect formation energy in AlN layers.^[14,15] A similar result in unintentional doping under continuously grown AlGaN-based layers due to SiC carrier decomposition is reported by Jeschke et al.^[23] A solution to this unintentional silicon incorporation might be to switch to TaC carriers, which have a higher temperature stability compared to SiC, as also suggested by Jeschke et al.^[23]

Finally, the concentrations of oxygen are found to vary substantially across the samples but are the highest in samples C2 and C2*. The low vapor supersaturation during the growth of sample C2 leads to an increase in oxygen concentration, but a clear maximum is observed in sample C2*. The increase in O concentration is expected in sample C2*, as N-polar domains in the introduced mixed-polar layer are known to favor significant incorporation of oxygen.^[21] We thus propose the observed high-energetic absorption band peaking below 245 nm in Figure 3 to be induced by an O-related defect state, inducing significant absorption only for O concentrations above 10^{18} cm^{-3} . The absorption coefficients determined for the high absorbing AlN samples P and C2* deposited by MOCVD lie around 1000 cm^{-1} and are therefore in good agreement with reported values of AlN films grown by MOCVD with near-identical impurity concentrations of oxygen and carbon.^[16] The results are also consistent with alternative AlN deposition techniques such as PVT and HVPE.^[14,15] Thus, we propose that the most frequently used deposition techniques for AlN all suffer from similar absorption issues in the UV-C spectral region, caused by carbon and oxygen incorporation.

We conclude our study by briefly discussing potential defect configurations and transitions responsible for the absorption and emission bands observed in Figure 1–4. We already determined that the absorption band centered around 265 nm observed in sample P is caused by carbon, typically introduced as a substitute atom on a nitrogen site, i.e., C_N .^[14] The defect luminescence observed in sample P and (slightly shifted in energy position due to the lower carbon concentration) samples

C1 and C2 may be attributed to radiative transitions from the conduction band (3.9 eV, $\text{CB} \rightarrow \text{C}_\text{N}$) and nitrogen vacancies (2.8 eV, $\text{V}_\text{N}^+ \rightarrow \text{C}_\text{N}$) to the carbon substitute defects.^[24] Concerning sample C2*, the high-energy absorption band exceeding our measurement range and peaking below 245 nm was identified as oxygen-related, which may be incorporated in a multitude of different defect states. Potential candidates for the PL emission at 3.3 eV are transitions from an O-DX center to the valence band ($\text{O} - \text{DX} \rightarrow \text{VB}$) and from O substituted on a nitrogen site to an uncharged complex consisting of the same defect state complemented by an aluminum vacancy ($\text{O}_\text{N} \rightarrow \text{V}_\text{Al} - \text{O}_\text{N}$).^[24]

4. Conclusions

In conclusion, we performed optical absorption and PL measurements on AlN epitaxial layers grown by MOCVD on sapphire. We found that, in general, low vapor supersaturation growth conditions by increased process temperature or pulsed growth mode significantly promotes the incorporation of point defects. In particular, NH_3 pulsing during epitaxial growth dramatically enhances the absorption coefficient in the UV-C spectral region. Two different absorption bands were observed and the point defect types responsible could unambiguously be identified. The sample grown using NH_3 pulsing exhibited a strong absorption band centered at 265 nm, caused by enhanced carbon incorporation, while samples grown with higher and even lower vapor supersaturation using a continuous growth mode contained a significantly lower concentration of defects and showed only weak absorption in the energy range studied. When switching the AlN nucleation layer from III-polar to a more N-polar biased growth (mixed-polar film), a different, high-energetic absorption band peaking below 245 nm emerges. As inversion domains themselves favor the incorporation of oxygen, the absorption band could be allocated to oxygen, as further evidenced by SIMS measurements. Therefore, heteroepitaxial MOCVD-grown AlN epitaxial layers suffer from similar issues in terms of impurity incorporation compared to their HVPE- and PVT-grown counterparts, highlighting the possible compatibility of the results obtained by experiments on either growth technique. Our results in terms of point defect incorporation in heteroepitaxial-grown AlN by MOCVD, depending on growth mode and kinetics, allow for a crucial choice of AlN growth parameters to provide highly transparent templates for UV-C LEDs processed in a flip-chip configuration by inhibiting occurring absorption bands at the desired emission wavelength.

Acknowledgements

N.T. and C.F. contributed equally to this work. A part of this work was funded by the German Federal Ministry of Economic Affairs (Bundesministerium für Wirtschaft und Energie) in the frame of the "Important Project of Common European Interest (IPCEI) on Microelectronics" (16IPCEI623). Furthermore, this work was supported by the German Federal Ministry of Education and Research (BMBF) within the "Advanced UV for Life" project (03ZZ0134A), by the German Science Foundation (DFG) within the Collaborative Research Center 787 (CRC787) as well as under Germany's Excellence Strategy labeled EXC-2123 QuantumFrontiers 390837967. Open-access funding enabled and organized by Projekt DEAL.

Conflict of Interest

The authors declare no conflict of interest.

Keywords

absorption, AlN, epitaxy, metal-organic chemical vapor deposition, point defects

Received: May 22, 2020

Revised: July 16, 2020

Published online: August 18, 2020

- [1] M. Stibich, J. Stachowiak, B. Tanner, M. Berkheiser, L. Moore, I. Raad, R. F. Chemaly, *Infect. Control Hosp. Epidemiol.* **2011**, 32, 3.
- [2] G. Y. Lui, D. Roser, R. Corkish, N. J. Ashbolt, R. Stuetz, *Sci. Total Environ.* **2016**, 553, 626.
- [3] K. Song, M. Mohseni, F. Taghipour, *Water Res.* **2016**, 94, 341.
- [4] T. Wang, S. J. MacGregor, J. G. Anderson, G. A. Woolsey, *Water Res.* **2005**, 39, 2921.
- [5] G. Messina, S. Burgassi, D. Messina, V. Montagnani, G. Cevenini, *Am. J. Infect. Control* **2015**, 43, 61.
- [6] S. E. Beck, R. A. Rodriguez, M. A. Hawkins, T. M. Hargy, T. C. Larason, K. G. Linden, *Appl. Environ. Microbiol.* **2016**, 82, 5.
- [7] A. Pandey, W. J. Shin, J. Gim, R. Hovden, Z. Mi, *Photonics Res.* **2020**, 8, 3.
- [8] T. Takano, T. Mino, J. Sakai, N. Noguchi, K. Tsubaki, H. Hirayama, *Appl. Phys. Express* **2017**, 10, 031002.
- [9] H. Hirayama, N. Maeda, S. Fujikawa, S. Toyoda, N. Kamata, *Jpn. J. Appl. Phys.* **2014**, 53, 100209.
- [10] P. Pampili, P. J. Parbrook, *Mater. Sci. Semicond. Process.* **2017**, 62, 180.
- [11] Y. Nagasawa, A. Hirano, *Appl. Sci.* **2018**, 8, 1264.
- [12] W. M. Yim, E. J. Stofko, P. J. Zanzucchi, J. I. Pankove, M. Ettenberg, S. L. Gilbert, *J. Appl. Phys.* **1973**, 44, 292.
- [13] T. Mattila, R. M. Niemen, *Phys. Rev. B* **1997**, 55, 15.
- [14] R. Collazo, J. Xie, B. E. Gaddy, Z. Bryan, R. Kirste, M. Hoffmann, R. Dalmau, B. Moody, Y. Kumagai, T. Nagashima, Y. Kubota, T. Kinoshita, A. Koukitu, D. L. Irving, Z. Sitar, *Appl. Phys. Lett.* **2012**, 100, 191914.
- [15] D. Alden, J. S. Harris, Z. Bryan, J. N. Baker, P. Reddy, S. Mita, G. Callen, A. Hoffmann, D. L. Irving, R. Collazo, Z. Sitar, *Phys. Rev. Appl.* **2018**, 9, 054036.
- [16] K. Nagata, H. Makino, T. Yamamoto, Y. Saito, H. Miki, *Jpn. J. Appl. Phys.* **2019**, 58, SCCC29.
- [17] W. K. Burton, N. Cabrera, F. C. Frank, *Philos. Trans. R. Soc. A* **1951**, 243, 299.
- [18] S. Mita, R. Collazo, A. Rice, R. F. Dalmau, Z. Sitar, *J. Appl. Phys.* **2008**, 104, 013521.
- [19] I. Bryan, Z. Bryan, S. Mita, A. Rice, J. Tweedie, R. Collazo, Z. Sitar, *J. Cryst. Growth* **2016**, 438, 81.
- [20] N. Susilo, S. Hagedorn, D. Jaeger, H. Miyake, U. Zeimer, C. Reich, B. Neuschulz, L. Sulmoni, M. Guttman, F. Mehnke, C. Kuhn, T. Wernicke, M. Weyers, M. Kneissl, *Appl. Phys. Lett.* **2018**, 112, 041110.
- [21] R. Collazo, S. Mita, A. Rice, R. F. Dalmau, Z. Sitar, *Appl. Phys. Lett.* **2007**, 91, 212103.
- [22] Z. Bryan, I. Bryan, J. Xie, S. Mita, Z. Sitar, R. Collazo, *Appl. Phys. Lett.* **2015**, 106, 142107.
- [23] J. Jeschke, A. Knauer, M. Weyers, *J. Cryst. Growth* **2018**, 483, 297.
- [24] T. Koppe, H. Hofsäss, U. Vetter, *J. Lumin.* **2016**, 178, 267.